International Journal of Heat and Mass Transfer 52 (2009) 6021–6027

Contents lists available at ScienceDirect

International Journal of Heat and Mass Transfer

journal homepage: www.elsevier.com/locate/ijhmt

Heat transfer analysis of soil heating systems

C.C. Ngo [a], F.C. Lai [b,*]

[a] Department of Mechanical Engineering, University of North Dakota, Grand Forks, ND 58202, United States
[b] School of Aerospace and Mechanical Engineering, University of Oklahoma, 212 Felgar Hall, 865 Asp Avenue, Norman, OK 73019, United States

ARTICLE INFO

Article history:
Received 13 January 2009
Received in revised form 10 July 2009
Available online 16 September 2009

Keywords:
Natural convection
Porous media
Soil heating systems
Superimposed fluid layer

ABSTRACT

Heat transfer from a pipe in a soil heating system has been numerically examined in this study. The Brinkman-extended Darcy equations are used to model the flow in the soil while Navier–Stokes equations are used for that above the soil. A parametric study has been performed to investigate the effects of Rayleigh number, Darcy number, and air layer thickness on the flow patterns and heat transfer rates. The results show that heat transfer increases with the Rayleigh number, but the convective strength decreases with a reduction in the Darcy number. The present results confirm the existence of a critical fluid layer thickness that leads to a minimum heat transfer from the pipe. However, the critical layer thickness is a more complicated function of Rayleigh number and Darcy number than that reported in the previous studies.

1. Introduction

Heat transfer from a buried pipe is involved in many important engineering applications, which include power cables, underground pipelines for oil and gas transport, and the disposal of nuclear wastes. The problem considered in the present study has applications related to soil heating in agriculture as well as in-floor heating in residence and industry. These heating systems are often used in conjunction with solar or geothermal energy systems. To adequately model these heating systems, one needs to consider the interaction between the overlaying fluid layer and the porous medium in which a heated pipe is buried.

Heat transfer from a buried pipe has been considered for various modes and configurations [1–9]. However, most previous studies have not explicitly considered the interaction between the superimposed fluid layer and the porous medium in which the pipe is buried. To simplify the analysis, the previous studies have either assumed an impermeable interface [5–9] or applied a simplified condition at the permeable interface [3]. In either case, they completely ignored the effect of convection in the superimposed fluid layer. Although Oosthuizen and Naylor [8] included the interaction between the superimposed fluid layer and the porous medium in their analysis, they assumed an impermeable interface so that the interaction was limited to heat transfer only. For a pipe buried in a semi-infinite porous medium, Bau [3] has reported that there exists a critical buried depth that leads to minimal heat transfer from the pipe. On the other hand, Oosthuizen and Naylor [8] have reported the existence of a critical thickness of the superimposed fluid layer that minimizes the heat transfer rate from the pipe. Thus, another objective of the present study is to verify the validity of the above claims.

2. Formulation and numerical method

The geometry considered is a pipe with a radius of r_i buried horizontally in a soil layer at a depth of d (Fig. 1). A fluid layer (air) with a thickness of L is laid on top of the soil. The interface between the two layers is assumed permeable so that air is the common medium for heat and mass transfer involved. The top surface of the air layer is assumed impermeable and maintained at a constant temperature T_c while the buried pipe is maintained at a higher temperature T_h. The soil layer is assumed to saturate with air. For simplicity, the effect of moisture which may be present in air has been neglected in the current analysis.

Assume that the convective flow induced by the heated pipe is steady and two-dimensional. Thus the governing equations for the soil layer can be formulated by the Brinkman-extended Darcy equations [10–12]:

$$\frac{\partial u_1}{\partial x}+\frac{\partial v_1}{\partial y}=0, \tag{1}$$

$$\frac{\partial p_1}{\partial x}=-\frac{\mu_1}{K}u_1+\tilde{\mu}\left(\frac{\partial^2 u_1}{\partial x^2}+\frac{\partial^2 u_1}{\partial y^2}\right)-\rho_1\left(u_1\frac{\partial u_1}{\partial x}+v_1\frac{\partial u_1}{\partial y}\right), \tag{2}$$

$$\frac{\partial p_1}{\partial y}=-\frac{\mu_1}{K}v_1-\rho_1 g+\tilde{\mu}\left(\frac{\partial^2 v_1}{\partial x^2}+\frac{\partial^2 v_1}{\partial y^2}\right)-\rho_1\left(u_1\frac{\partial v_1}{\partial x}+v_1\frac{\partial v_1}{\partial y}\right), \tag{3}$$

$$u_1\frac{\partial T_1}{\partial x}+v_1\frac{\partial T_1}{\partial y}=\alpha_1\left[\frac{\partial^2 T_1}{\partial x^2}+\frac{\partial^2 T_1}{\partial y^2}\right]. \tag{4}$$

* Corresponding author.
E-mail address: flai@ou.edu (F.C. Lai).

0017-9310/$ - see front matter © 2009 Elsevier Ltd. All rights reserved.
doi:10.1016/j.ijheatmasstransfer.2009.07.011

Nomenclature

c_p	specific heat [kJ/kg K]	T	temperature [K]
Da	Darcy number K/r_i^2	u, v	velocity in the x- and y-direction [m/s]
d	buried depth [m]	x, y	Cartesian coordinates [m]
g	gravitational acceleration [m/s^2]	w	width of the physical domain [m]
h	heat transfer coefficient [W/m^2 K]	α	thermal diffusivity, $k/\rho c_p$ [m^2/s]
K	permeability [m^2]	β	coefficient of thermal expansion [1/K]
k	thermal conductivity [W/m K]	η	body-fitted coordinate
L	thickness of the superimposed fluid layer [m]	Θ	dimensionless temperature, $(T\text{-}T_c)/(T_h\text{-}T_c)$
Nu	Nusselt number, hr_i/k	μ	dynamic viscosity [kg/m s]
P	grid control function	$\tilde{\mu}$	effective viscosity [kg/m s]
Pr	Prandtl number, v/α	v	kinematic viscosity [m^2/s]
p	pressure [N/m^2]	ρ	density [kg/m^3]
Q	grid control function	ξ	body-fitted coordinate
r_i	radius of buried pipe [m]	Ψ	dimensionless stream function
Ra	Rayleigh number, $g\beta(T_h\text{-}T_c)r_i^3/\alpha v$	Ω	dimensionless vorticity

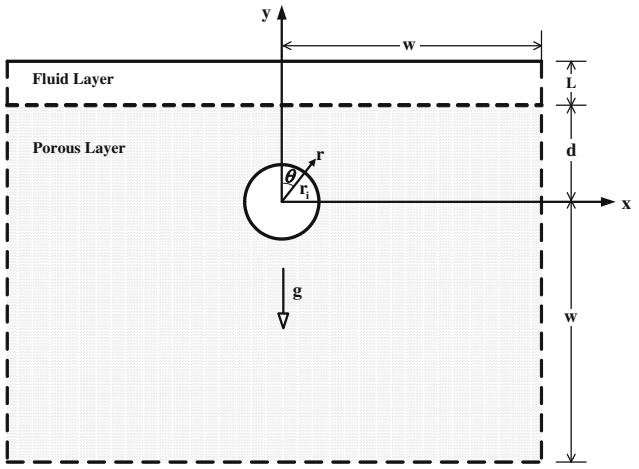

Fig. 1. A pipe buried horizontally in a semi-infinite soil with a superimposed air layer.

The governing equations for the fluid layer are the Navier–Stokes equations:

$$\frac{\partial u_2}{\partial x}+\frac{\partial v_2}{\partial y}=0, \tag{5}$$

$$\frac{\partial p_2}{\partial x}=\mu_2\left(\frac{\partial^2 u_2}{\partial x^2}+\frac{\partial^2 u_2}{\partial y^2}\right)-\rho_2\left(u_2\frac{\partial u_2}{\partial x}+v_2\frac{\partial u_2}{\partial y}\right), \tag{6}$$

$$\frac{\partial p_2}{\partial y}=-\rho_2 g+\mu_2\left(\frac{\partial^2 v_2}{\partial x^2}+\frac{\partial^2 v_2}{\partial y^2}\right)-\rho_2\left(u_2\frac{\partial v_2}{\partial x}+v_2\frac{\partial v_2}{\partial y}\right), \tag{7}$$

$$u_2\frac{\partial T_2}{\partial x}+v_2\frac{\partial T_2}{\partial y}=\alpha_2\left[\frac{\partial^2 T_2}{\partial x^2}+\frac{\partial^2 T_2}{\partial y^2}\right], \tag{8}$$

where the subscripts 1 and 2 denote the soil and fluid layers, respectively. The effective viscosity that appears in the Brinkman term (Eqs. (2) and (3)) is assumed to be the same as the fluid viscosity (i.e., $\tilde{\mu}=\mu$). In line with Boussinesq approximation (Eq. (9)), the variation of density is only accounted for in the buoyancy term. All other thermophysical properties are assumed constant.

$$\rho\approx\rho_c[1-\beta(T-T_c)]. \tag{9}$$

Since the physical domain is symmetrical, only one half of the domain [$-w\leqslant x\leqslant 0$ and $-w\leqslant y\leqslant(d+L)$] is considered for computations. Thus, the boundary conditions are given by

$$\text{At } r=r_i,\quad \pi\leq\theta\leq 2\pi,\quad T_1=T_h,\quad u_{r1}=0. \tag{10a}$$

$$\text{At } y=(d+L),\quad -w\leq x\leq 0,\quad T_2=T_c,\quad u_2=v_2=0. \tag{10b}$$

$$\text{At } x=-w,\quad -w\leq y\leq d,\quad \frac{\partial T_1}{\partial x}=0,\quad v_1=0.$$

$$d\leq y\leq(d+L),\quad \frac{\partial T_2}{\partial x}=0,\quad v_2=0. \tag{10c}$$

$$\text{At } y=-w,\quad -w\leq x\leq 0,\quad \frac{\partial T_1}{\partial y}=0\quad u_1=0. \tag{10d}$$

$$\text{At } x=0,\quad r_i\leq y\leq d,\quad \frac{\partial T_1}{\partial x}=0,\quad u_1=0.$$

$$d\leq y\leq(d+L),\quad \frac{\partial T_2}{\partial x}=0,\quad u_2=0.$$

$$-r_i\leq y\leq -w,\quad \frac{\partial T_1}{\partial x}=0,\quad u_1=0. \tag{10e}$$

Boundary conditions (10c) and (10d) imply that heat and fluid flow far away from the pipe are negligibly small if the domain considered is sufficiently large. No-slip condition is applied at the impermeable top boundary. In addition to the boundary conditions, appropriate conditions need to be specified at the interface between the fluid and porous regions. The interface conditions applied in the present study are the continuity of temperature, heat flux, normal and tangential velocity, shear stress and pressure [10–14]:

$$T_1=T_2, \tag{11a}$$

$$k_1\frac{\partial T_1}{\partial y}=k_2\frac{\partial T_2}{\partial y}, \tag{11b}$$

$$u_1=u_2, \tag{11c}$$

$$v_1=v_2, \tag{11d}$$

$$\mu_1\left(\frac{\partial v_1}{\partial x}+\frac{\partial u_1}{\partial y}\right)=\mu_2\left(\frac{\partial v_2}{\partial x}+\frac{\partial u_2}{\partial y}\right), \tag{11e}$$

$$p_1=p_2. \tag{11f}$$

Due to the complexity of the geometry involved, body-fitted coordinates have been employed [15–16]. A computational grid used for the present study is shown in Fig. 2. The governing equations (Eqs. (1)–(8)) along with the boundary conditions (Eqs. (10a)–(10e)) and interface conditions (Eqs. (11a)–(11f)) are transformed to the computational domain accordingly.

After introducing the stream functions and vorticity, the dimensionless governing equations for the porous layer are given by:

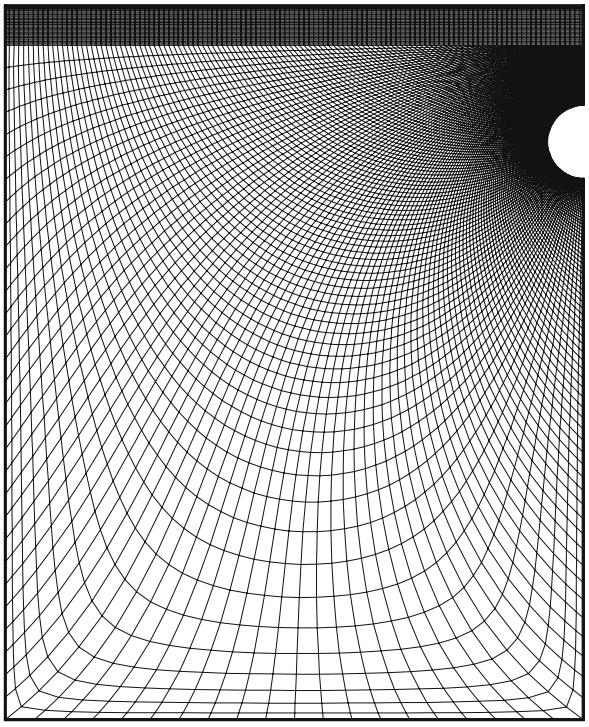

Fig. 2. Computational grid for the present study.

$$\nabla^2_{\xi\eta}\Psi_1 = -\Omega_1, \tag{12}$$

$$\nabla^2_{\xi\eta}\Omega_1 = \frac{\Omega_1}{Da} - \frac{Ra}{J}\left[\frac{\partial\Theta_1}{\partial\xi}\frac{\partial Y}{\partial\eta} - \frac{\partial\Theta_1}{\partial\eta}\frac{\partial Y}{\partial\xi}\right] + \frac{1}{Pr\cdot J}\left[\frac{\partial\Omega_1}{\partial\xi}\frac{\partial\Psi_1}{\partial\eta} - \frac{\partial\Omega_1}{\partial\eta}\frac{\partial\Psi_1}{\partial\xi}\right], \tag{13}$$

$$\nabla^2_{\xi\eta}\Theta_1 = \frac{\alpha_2}{\alpha_1}\frac{1}{J}\left[\frac{\partial\Theta_1}{\partial\xi}\frac{\partial\Psi_1}{\partial\eta} - \frac{\partial\Theta_1}{\partial\eta}\frac{\partial\Psi_1}{\partial\xi}\right]. \tag{14}$$

For the fluid layer, they are

$$\nabla^2_{\xi\eta}\Psi_2 = -\Omega_2, \tag{15}$$

$$\nabla^2_{\xi\eta}\Omega_2 = -\frac{Ra}{J}\left[\frac{\partial\Theta_2}{\partial\xi}\frac{\partial Y}{\partial\eta} - \frac{\partial\Theta_2}{\partial\eta}\frac{\partial Y}{\partial\xi}\right] + \frac{1}{Pr\cdot J}\left[\frac{\partial\Omega_2}{\partial\xi}\frac{\partial\Psi_2}{\partial\eta} - \frac{\partial\Omega_2}{\partial\eta}\frac{\partial\Psi_2}{\partial\xi}\right], \tag{16}$$

$$\nabla^2_{\xi\eta}\Theta_2 = \frac{1}{J}\left[\frac{\partial\Theta_2}{\partial\xi}\frac{\partial\Psi_2}{\partial\eta} - \frac{\partial\Theta_2}{\partial\eta}\frac{\partial\Psi_2}{\partial\xi}\right], \tag{17}$$

where

$$\nabla^2_{\xi\eta} = \frac{\alpha}{J^2}\frac{\partial^2}{\partial\xi^2} - \frac{2\beta}{J^2}\frac{\partial^2}{\partial\xi\partial\eta} + \frac{\gamma}{J^2}\frac{\partial^2}{\partial\eta^2} + P\frac{\partial}{\partial\xi} + Q\frac{\partial}{\partial\eta}, \tag{18}$$

is the Laplacian operator in the transformed domain. α, β, and γ are the transformation coefficients while J is the Jacobian, P and Q are the grid control functions. The governing parameters are the Darcy number ($Da = K/r_i^2$), Rayleigh number ($Ra = g\beta(T_h - T_c)r_i^3/\alpha\nu$) and Prandtl number ($Pr = \nu/\alpha$). Air ($Pr = 0.7$) is the working fluid considered in the present study.

Similarly, the boundary conditions (Eqs. (10a)–(10e)) in the transformed domain are given by

$$\text{At } \eta = \eta_o, \quad \xi_o \le \xi \le \xi_m, \quad \Theta_1 = 1, \quad \Psi_1 = 0. \tag{19a}$$

$$\text{At } \eta = \eta_n, \quad \xi_o \le \xi \le \xi_m, \quad \Theta_2 = 0, \quad \Psi_2 = 0. \tag{19b}$$

$$\text{At } \xi = \xi_o, \quad \eta_o \le \eta \le \eta_1, \quad \frac{\partial\Theta_1}{\partial\xi}\frac{\partial Y}{\partial\eta} - \frac{\partial\Theta_1}{\partial\eta}\frac{\partial Y}{\partial\xi} = 0, \quad \Psi_1 = 0.$$

$$\eta_1 \le \eta \le \eta_2, \quad \frac{\partial\Theta_1}{\partial\xi}\frac{\partial X}{\partial\eta} - \frac{\partial\Theta_1}{\partial\eta}\frac{\partial X}{\partial\xi} = 0,$$

$$\frac{\partial\Psi_1}{\partial\xi}\frac{\partial X}{\partial\eta} - \frac{\partial\Psi_1}{\partial\eta}\frac{\partial X}{\partial\xi} = 0.$$

$$\eta_2 \le \eta \le \eta_{\text{int}}, \quad \frac{\partial\Theta_1}{\partial\xi}\frac{\partial Y}{\partial\eta} - \frac{\partial\Theta_1}{\partial\eta}\frac{\partial Y}{\partial\xi} = 0,$$

$$\frac{\partial\Psi_1}{\partial\xi}\frac{\partial Y}{\partial\eta} - \frac{\partial\Psi_1}{\partial\eta}\frac{\partial Y}{\partial\xi} = 0.$$

$$\eta_{\text{int}} \le \eta \le \eta_n, \quad \frac{\partial\Theta_2}{\partial\xi}\frac{\partial Y}{\partial\eta} - \frac{\partial\Theta_2}{\partial\eta}\frac{\partial Y}{\partial\xi} = 0,$$

$$\frac{\partial\Psi_2}{\partial\xi}\frac{\partial Y}{\partial\eta} - \frac{\partial\Psi_2}{\partial\eta}\frac{\partial Y}{\partial\xi} = 0. \tag{19c}$$

$$\text{At } \xi = \xi_m, \quad \eta_o \le \eta \le \eta_{\text{int}}, \quad \frac{\partial\Theta_1}{\partial\xi}\frac{\partial Y}{\partial\eta} - \frac{\partial\Theta_1}{\partial\eta}\frac{\partial Y}{\partial\xi} = 0, \quad \Psi_1 = 0.$$

$$\eta_{\text{int}} \le \eta \le \eta_n, \quad \frac{\partial\Theta_2}{\partial\xi}\frac{\partial Y}{\partial\eta} - \frac{\partial\Theta_2}{\partial\eta}\frac{\partial Y}{\partial\xi} = 0, \quad \Psi_2 = 0. \tag{19d}$$

where the subscript "int" refers to the location of the interface.

The transformed interface conditions (Eqs. (11a)–(11f)) are

$$\Theta_1 = \Theta_2, \tag{20a}$$

$$\frac{\partial\Theta_1}{\partial\xi}\frac{\partial X}{\partial\eta} - \frac{\partial\Theta_1}{\partial\eta}\frac{\partial X}{\partial\xi} = \frac{\alpha_2}{\alpha_1}\left[\frac{\partial\Theta_2}{\partial\xi}\frac{\partial X}{\partial\eta} - \frac{\partial\Theta_2}{\partial\eta}\frac{\partial X}{\partial\xi}\right], \tag{20b}$$

$$\frac{\partial\Psi_1}{\partial\xi}\frac{\partial X}{\partial\eta} - \frac{\partial\Psi_1}{\partial\eta}\frac{\partial X}{\partial\xi} = \frac{\partial\Psi_2}{\partial\xi}\frac{\partial X}{\partial\eta} - \frac{\partial\Psi_2}{\partial\eta}\frac{\partial X}{\partial\xi}, \tag{20c}$$

$$\Psi_1 = \Psi_2, \tag{20d}$$

$$\Omega_1 = \Omega_2, \tag{20e}$$

$$\frac{\partial\Omega_1}{\partial\xi}\frac{\partial X}{\partial\eta} - \frac{\partial\Omega_1}{\partial\eta}\frac{\partial X}{\partial\xi} + \frac{1}{Da}\left[\frac{\partial\Psi_1}{\partial\xi}\frac{\partial X}{\partial\eta} - \frac{\partial\Psi_1}{\partial\eta}\frac{\partial X}{\partial\xi}\right] = \frac{\partial\Omega_2}{\partial\xi}\frac{\partial X}{\partial\eta} - \frac{\partial\Omega_2}{\partial\eta}\frac{\partial X}{\partial\xi}. \tag{20f}$$

The governing equations along with the boundary conditions are solved by finite difference method [9,16]. The interface conditions are implemented using imaginary nodes as described by Rana et al. [17]. For the present study, the dimensionless buried depth of the pipe is fixed at five ($d/r_i = 5$) while the fluid layer thicknesses is varied ($0.5 \leqslant L/r_i \leqslant 3.5$). From our previous work [9], it has been found that a dimensionless width (w/r_i) of 30 is sufficient to represent a semi-infinite medium. In addition, a uniform grid of 121×151 in the transformed domain (121×121 for the porous medium and 121×31 for the superimposed fluid layer) offers the best results in terms of the computational efficiency and accuracy. It should be noted that a further increase in the refinement does not produce any significant improvement in the heat transfer results. As an additional check on the accuracy of the numerical results, an overall energy balance has been performed after each calculation, which yields a relative error of less than 3%.

3. Results and discussion

A parametric study has been performed over a wide range of the governing parameters (i.e., $0.5 \leqslant L/r_i \leqslant 3.5$, $0.0005 \leqslant Da \leqslant 0.05$, and $10^3 \leqslant Ra \leqslant 10^5$) for air ($Pr = 0.7$).

3.1. Effects of thermal buoyancy

The effects of thermal buoyancy (i.e., the Rayleigh number) on the flow and temperature fields can be examined from Fig. 3. For a better observation of the flow structure and temperature field, results are only presented for region in the vicinity of the pipe ($-15 \leqslant X \leqslant 0$, $-10 \leqslant Y \leqslant 7$). At $Ra = 10^3$, the flow field is dominated

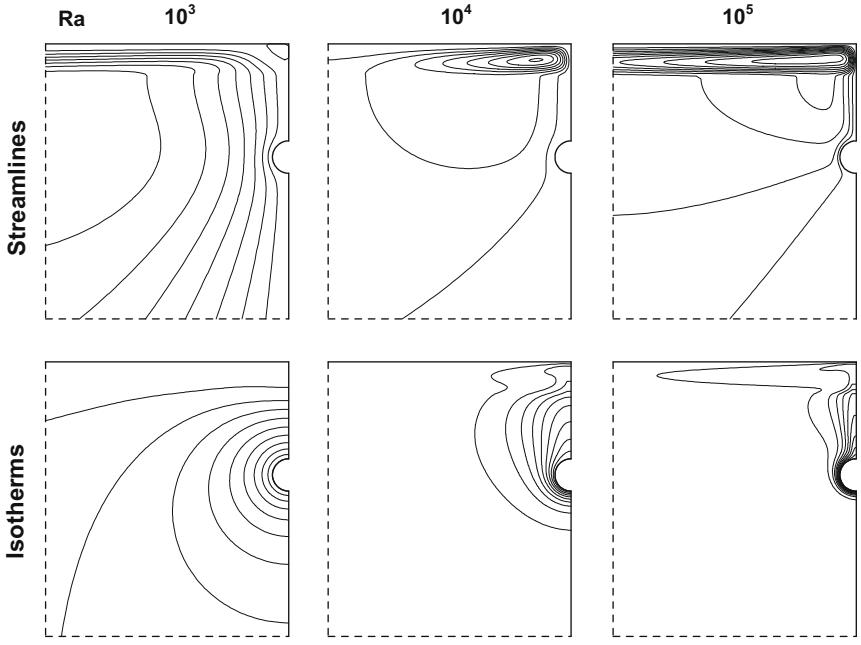

Fig. 3. Effects of Rayleigh number on the flow and temperature fields of a saturated soil layer with a superimposed air layer of $L/r_i = 2$ ($Da = 0.0005$, $\Delta\Theta = 0.1$; $\Delta\Psi = 0.1$, 2, and 5 for $Ra = 10^3$, 10^4, and 10^5, respectively).

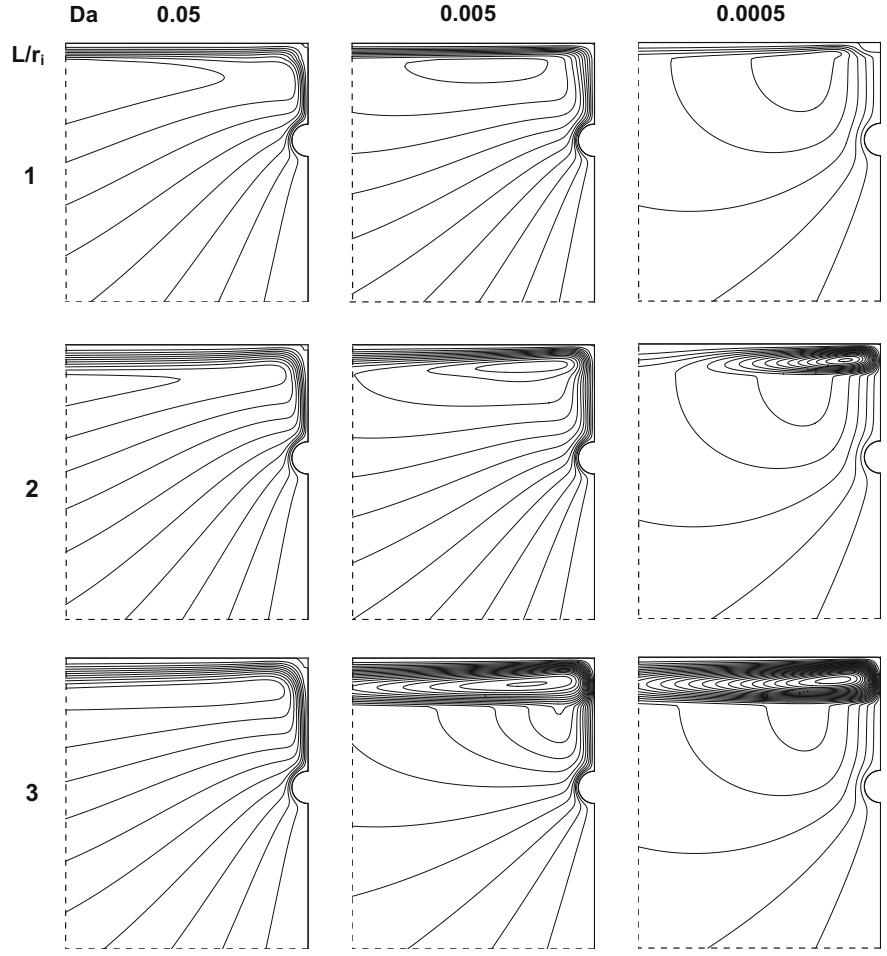

Fig. 4. Effects of the thickness of a superimposed air layer and Darcy number on the flow fields for $Ra = 10^4$ ($\Delta\Psi = 5$, 2, and 1 for $Da = 0.05$, 0.005, and 0.0005, respectively).

by a primary flow which constitutes of heated fluid rising along the pipe wall to the top boundary and returning from the left boundary when it is cooled. Also, there is a secondary flow, a small recirculating cell, which is formed within the air layer near the top of

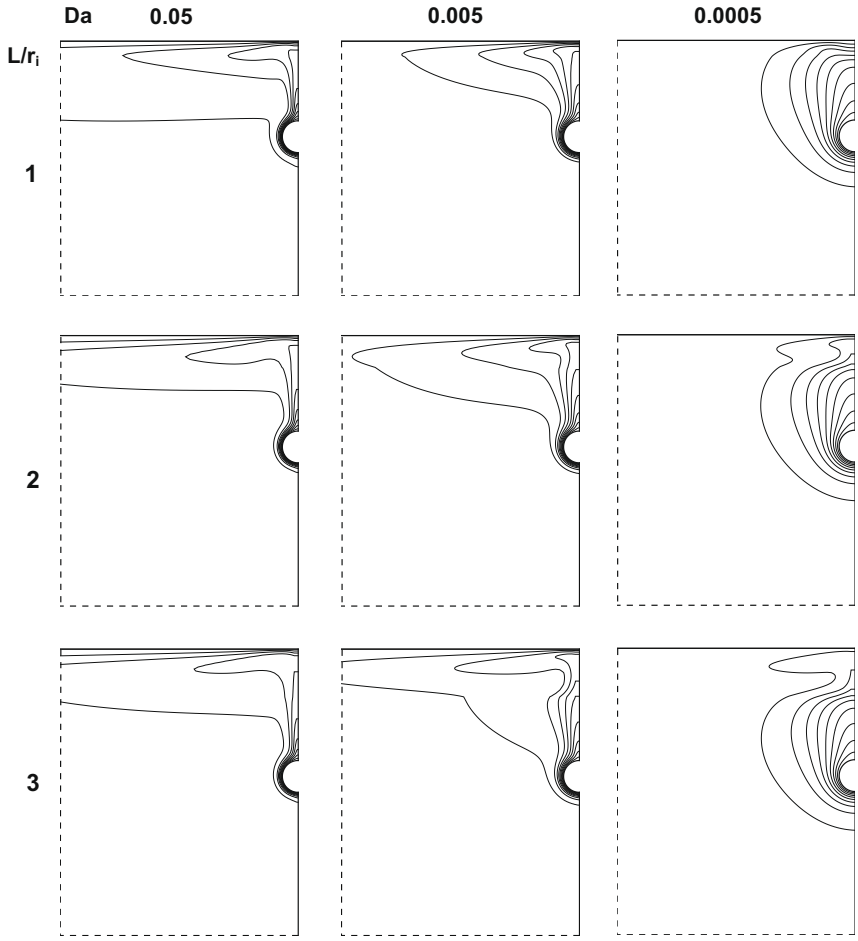

Fig. 5. Effects of the thickness of a superimposed air layer and Darcy number on the temperature fields for $Ra = 10^4$ ($\Delta\Theta = 0.1$).

the pipe. The overall strength of convection is weak and heat transfer remains in the conduction mode, which is evident from the nearly concentric isotherms displayed in the figure.

As the Rayleigh number increases, convection is further developed and the flow field is prevailed by a single large cell with the eye of the cell mainly confined in the air layer. Notice that the streamlines in Fig. 3 are plotted using a larger interval for a higher Rayleigh number (i.e., $\Delta\Psi = 0.1$, 2, and 5 for $Ra = 10^3$, 10^4, and 10^5, respectively) for better observation of the flow structure in the fluid layer. Also, it is noticed that due to a large flow resistance in the soil layer, the convective cell is confined mostly in the air layer. From the isotherms, the development of thermal boundary layer around the pipe can be clearly observed. With an increase in the Rayleigh number, a steeper temperature gradient can be observed at the lower part of the pipe. In addition, the formation of a thermal plume near the top of the pipe can be observed as the Rayleigh number increases. The isotherms within the air layer are perturbed due to the formation of recirculating cell.

3.2. Effects of air layer thickness and Darcy number

The effects of the superimposed air layer thickness and Darcy number on the flow and temperature fields are shown in Figs. 4 and 5. Recall that the Darcy number is defined as K/r_i^2. Thus, for a given pipe size, a large Darcy number implies that the soil layer is more permeable. For a given Rayleigh number, it is observed that the strength of the convective cell increases with an increase in the air layer thickness. In these cases, the air layer acts as a reservoir to continuously supply air to the soil layer to sustain the convection. As the Darcy number decreases from 0.05 to 0.0005, the primary flow structure remains the same, but the overall strength of the convective flow decreases due to the added flow resistance in the soil layer, which is also evident from the absence of a vigorous thermal plume in the temperature field (Fig. 5). However, a thicker air layer does produce a more noticeable effect of thermal buoyancy. It is interesting to observe that the eye of convective cell always resides in the soil layer for $L/r_i \leqslant 1$ and it moves inside the air layer only when $L/r_i > 1$. From Fig. 5, the presence of a vigorous thermal plume on top of the heated pipe can be clearly observed

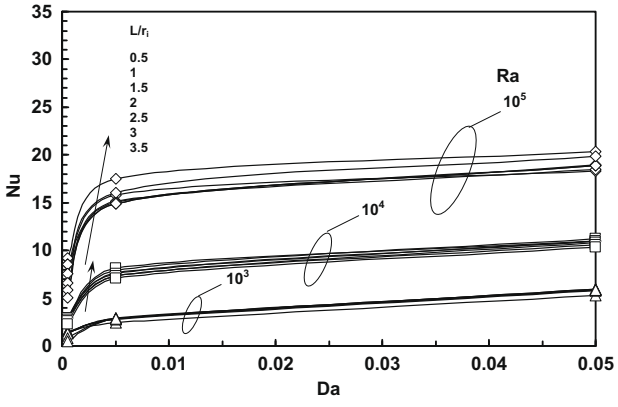

Fig. 6. Heat transfer results as a function of Darcy number.

for $Da \geqslant 0.005$, which further confirms that the flow field is highly convective when the soil layer is more permeable.

The effects of the air layer thickness and Darcy number on the flow and temperature fields follow a similar trend when the Rayleigh number increases to 10^5. For all Darcy numbers, the strength of convective flow becomes more pronounced with an increase in the Rayleigh number.

When comparing the flow fields obtained from the present study with those of Oosthuizen and Naylor [8] with an impermeable interface, one notices that the major difference between these two results is the formation of multi-cellular convection in the upper fluid layer in the latter case. Because of the impermeable interface, fluids on each side are not communicating and the re-circulating cells in the upper fluid layer are formed independently from the fluid in the lower porous layer. Accordingly, one observes two separately formed thermal plumes in the temperature field [8]. Due to the distinct differences observed, heat transfer results from these two studies also differ significantly as will be discussed in the following section.

3.3. Heat transfer results

The heat transfer results obtained from the present study are evaluated in terms of the Nusselt number at the top boundary, which is defined as

$$Nu = -\int_{-w/r_i}^{0} \left.\frac{\partial \Theta_2}{\partial Y}\right|_{Y=(L+d)/r_i} dX. \tag{21}$$

The Nusselt number thus defined also represents the total heat flux through the top boundary. By conservation of energy, this also equals to the total heat flux dissipated from the pipe. The variation of Nusselt numbers is shown in Fig. 6 as a function of the Darcy number. As expected, the heat transfer rate increases with the strength of thermal buoyancy (i.e., the Rayleigh number). It is observed that Nusselt number can increase as high as five times when Rayleigh number increases from 10^3 to 10^5. For a given Rayleigh number, it is observed that Nusselt number increases most rapidly when the Darcy number increases from 0.0005 to 0.005 whereas the rate of increase (i.e., the slope) is not as steep when the Darcy number increases further to 0.05. Also observed, the difference in the heat transfer rate among various air layer thicknesses is not significant at a low Rayleigh number, but becomes substantial when the Rayleigh number increases.

To better analyze the heat transfer variation with the thickness of superimposed air layer, Nusselt number is plotted as a function of dimensionless layer thickness L/r_i in Fig. 7. At a low Rayleigh number of 10^3 (Fig. 7(a)), the Nusselt number appears to increase slightly as L/r_i increases from 0.5 to 1, it then levels off with a further increase in L/r_i for $Da = 0.05$ but reduces for $Da = 0.005$ and 0.0005. At $Ra = 10^4$, one observes that the Nusselt number continues to decrease with an increase in the air layer thickness L/r_i (Fig. 7(b)). For $Ra = 10^5$, the variation of Nusselt number with air layer thickness becomes more complicated (Fig. 7(c)). For Da = 0.05 and 0.005, the Nusselt number first decreases with an increase in the air layer thickness. After it reaches a minimum, it begins to increase again with the air layer thickness. On the other hand, for $Da = 0.0005$, the Nusselt number continues to decrease with the air layer thickness and does not reach a minimal value for the air layer thickness range considered in the present study.

It has been reported by Oosthuizen and Naylor [8] that there exists a critical fluid layer thickness that leads to a minimum heat transfer rate from the buried pipe. Based on the results they obtained, the critical thickness of the superimposed fluid layer L/r_i lies between 1 and 2. From the present study, our results show that for $Ra = 10^5$ and $Da = 0.05$, a minimum Nusselt number was indeed found in the same range of the fluid layer thickness. However, for other Rayleigh and Darcy numbers, our results suggest that the critical fluid layer thickness, when exists, would lie outside the range previously reported (i.e., $L/r_i > 2$). Clearly, the difference in the prediction of the critical fluid layer thickness is due to the nature of the interface (i.e., permeable vs. impermeable). Since the interface is more likely to be permeable for most applications, the prediction from the present results should be more useful. Particularly, the result in Fig. 7(c) has suggested that the critical air layer thickness increases with a reduction in the permeability of soil.

4. Conclusion

Heat transfer by natural convection from a pipe buried horizontally in semi-infinite soil with a superimposed air layer has been numerically examined in this study. The effects of Rayleigh number, Darcy number, and air layer thickness on the heat transfer results have been investigated. The present result shows that heat dissipation from the pipe decreases when the soil becomes less permeable. Also, a critical air layer thickness appears to exist that leads to a minimum heat transfer from the pipe. For specific applications in soil or in-floor heating, this is to be avoided. Because of the difference in the nature of the interface, the critical air layer thickness predicted from the present study is greater than that from the previous study. The present result has further shown that the critical air layer thickness is a complicated function of the Ray-

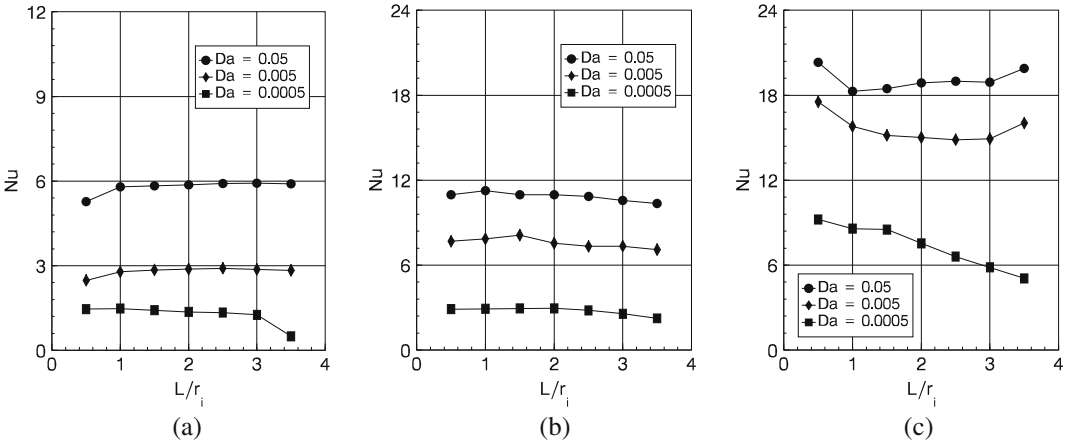

Fig. 7. Heat transfer results as a function of the air layer thickness L/r_i for (a) $Ra = 10^3$, (b) $Ra = 10^4$, and (c) $Ra = 10^5$.

leigh number and Darcy number. It suggests that the critical air layer thickness increases with a reduction in the permeability of the soil layer for a given Rayleigh number.

While the present study has extended several earlier studies on heat transfer from a buried pipe with the consideration of both porous medium and superimposed fluid layer, the finding from the present study has an important implication for the application of soil or in-floor heating systems that an analysis of the complete system (which includes the porous medium and the superimposed fluid layer) is required to obtain reliable and more accurate heat transfer results. Previous analyses using only isolated porous medium (soil layer) with simplified interface condition may not be sufficient to obtain the complete heat transfer characteristics of a buried pipe, particularly for the prediction of minimum heat transfer and critical buried depth. Normally, the criterion for a critical fluid layer thickness can be easily met for applications in an open field. However, for applications in a limited enclosed space, one needs to make sure that the fluid layer is sufficiently thick to have a better heat transfer result.

References

[1] E.R.G. Eckert, R.M. Drake, Heat and Mass Transfer, McGraw-Hill, New York, 1959.
[2] R.T. Fernandez, V.E. Schrock, Natural convection from cylinders buried in a liquid-saturated porous medium, in: Proceedings of the International Heat Transfer Conference, Munich, vol. 2, pp. 335–340.
[3] H.H. Bau, Convective heat losses from a pipe buried in a semi-infinite porous medium, Int. J. Heat Mass Transfer 27 (1984) 2047–2056.
[4] R.M. Fand, T.E. Steinberger, P. Cheng, Natural convection heat transfer from a horizontal cylinder embedded in a porous medium, Int. J. Heat Mass Transfer 29 (1986) 119–133.
[5] B. Farouk, H. Shayer, Natural convection around a heated cylinder in a saturated porous medium, J. Heat Transfer 110 (1988) 642–648.
[6] K. Himasekhar, H.H. Bau, Thermal convection around a heat source embedded in a box containing a saturated porous medium, J. Heat Transfer 110 (1988) 649–654.
[7] D.M. Christopher, B.-X. Wang, Non-Darcy natural convection around a horizontal cylinder buried near the surface of a fluid-saturated porous medium, Int. J. Heat Mass Transfer 36 (1993) 3663–3669.
[8] P.H. Oosthuizen, D. Naylor, Natural convective heat transfer from a cylinder in an enclosure partly filled with a porous medium, Int. J. Numer. Methods Heat Fluid Flow 6 (1996) 51–63.
[9] C.C. Ngo, F.C. Lai, Effects of backfill on heat transfer from a buried pipe, J. Heat Transfer 127 (2005) 780–784.
[10] K. Vafai, C.L. Tien, Boundary and inertia effects on flow and heat transfer in porous media, Int. J. Heat Mass Transfer 26 (1981) 195–203.
[11] T. Nishimura, T. Takumi, M. Shiraishi, Y. Kawamura, H. Ozoe, Numerical analysis of natural convection in a rectangular enclosure horizontally divided into fluid and porous regions, Int. J. Heat Mass Transfer 29 (1986) 889–898.
[12] S.B. Sathe, W.–Q. Lin, T.W. Tong, Natural convection in enclosure containing an insulation with a permeable fluid–porous interface, Int. J. Heat Fluid Flow 9 (1988) 389–395.
[13] B. Alazmi, K. Vafai, Analysis of fluid flow and heat transfer interfacial conditions between a porous medium and a fluid layer, Int. J. Heat Mass Transfer 44 (2001) 1735–1749.
[14] D.A. Nield, Modeling fluid flow in saturated porous media and at interfaces, in: D.B. Ingham, I. Pop (Eds.), Transport Phenomena in Porous Media II, Pergamon, Oxford, 1988.
[15] J.F. Thompson, Z.U.A. Warsi, C.W. Mastin, Boundary-fitted coordinates systems for numerical solution of partial differential equations – a review, J. Comput. Phys. 47 (1982) 1–108.
[16] B.A. Yost, The Analysis of Fluid Flow/Solidification Problems in Arbitrarily Shaped Domains, Ph.D. Dissertation, University of Delaware, Newark, DE, 1984.
[17] R. Rana, R.N. Horne, P. Cheng, Natural convection in a multilayered geothermal reservoir, J. Heat Transfer 101 (1979) 411–416.